Acta Oceanol. Sin., 2025, Vol. 44, No. 4, P. 35–47
https://doi.org/10.1007/s13131-024-2455-z

Influence of austral summer sea ice melting timing on particle fluxes and composition in Prydz Bay, East Antarctica

Changfeng Zhu[1], Yufei Ding[1], Wenhao Huang[1], Jun Zhao[1*], Dong Li[1], Haifeng Zhang[1], Yanhong Xu[1], Cai Zhang[1], Ji Hu[1], Shunan Cao[2], Guangfu Luo[2], Yongming Sun[3], Haitao Ding[2], Wei Zhang[1], Weiping Sun[1], Jianming Pan[1], Jianfeng He[2]

[1] Key Laboratory of Marine Ecosystem Dynamics, Second Institute of Oceanography, Ministry of Natural Resources, Hangzhou 310012, China

[2] Polar Research Institute of China, Shanghai 200136, China

[3] Key Laboratory of Physical Oceanography, Ministry of Education, Ocean University of China, Qingdao 266003, China

Received 14 October 2024; accepted 21 January 2025

© Chinese Society for Oceanography and Springer-Verlag GmbH Germany, part of Springer Nature 2025

Abstract

The melting of seasonal sea ice in Antarctica plays a pivotal role in the region's carbon cycle, influencing global carbon storage and the exchange of carbon between the atmosphere and the ocean. However, the impact of variability in the timing of seasonal sea ice retreat on the flux and composition of sinking particulate matter remains to be elucidated. In this study, we deployed sediment traps in Prydz Bay during the austral summers of 2019/2020 and 2020/2021, noting that sea ice melting occurred approximately one and a half months earlier in the former summer compared to the latter. We analyzed sediment trap data, which included total mass flux (TMF), particulate organic carbon (POC), biogenic silica (BSi), particulate inorganic carbon, and lithogenic particle (Litho) fluxes, as well as the stable isotopes $\delta^{13}C$ and $\delta^{15}N$ of particulate organic matter (POM). Additionally, we incorporated remote sensing data on sea ice concentration and chlorophyll *a*. This dramatic delay in sea ice melting timing could result in a significant increase in TMF, BSi and POC fluxes in the summer of 2020/2021 compared to 2019/2020. Elevated BSi fluxes and more ^{13}C-depleted POC in the austral summer of 2020/2021 suggest that the delayed melting of sea ice may have stimulated the productivity of centric diatoms. Furthermore, the higher BSi/POC ratio and more negative $\delta^{15}N$ values of POM, along with a reduced presence of krill in the traps, indicate a diminished grazing pressure from zooplankton, which collectively enhanced the sedimentation efficiency of POC during the austral summer of 2020/2021. These findings highlight the critical role of sea ice melting timing in regulating productivity, flux and composition of sinking particulate matter in the Prydz Bay ecosystem, with significant implications for carbon cycling in polar oceans.

Key words Prydz Bay, particle fluxes, sea ice melting timing, diatom, sediment trap

Citation Zhu Changfeng, Ding Yufei, Huang Wenhao, Zhao Jun, Li Dong, Zhang Haifeng, Xu Yanhong, Zhang Cai, Hu Ji, Cao Shunan, Luo Guangfu, Sun Yongming, Ding Haitao, Zhang Wei, Sun Weiping, Pan Jianming, He Jianfeng. 2025. Influence of austral summer sea ice melting timing on particle fluxes and composition in Prydz Bay, East Antarctica. Acta Oceanologica Sinica, 44(4): 35–47, doi: 10.1007/s13131-024-2455-z

1 Introduction

The seasonal ice zone (SIZ) of the Southern Ocean accounts for about 40% of the total area of the Southern Ocean (Roach et al., 2025) and serves as a significant area of high productivity there (Arrigo and van Dijken, 2003; Arrigo et al., 2015). As seasonal sea ice melts, there is an increase in light availability, the release of freshwater enriched with dissolved iron, and a subsequent decrease in the depth of the mixed layer (Lannuzel et al., 2007; Zhang

Foundation item: The National Key Research and Development Program of China under contract No. 2022YFE0136500; the Scientific Research Fund of the Second Institute of Oceanography, Ministry of Natural Resources, under contract Nos JG2212 and JG2211; the National Natural Science Foundation of China under contract Nos 42276255, 41976228, and 42176227; the National Polar Special Program "Impact and Response of Antarctic Seas to Climate Change" under contract Nos IRASCC 01-01-02 and IRASCC 02-02; the China Scholarship Council under contract No. 201704180017.

*Corresponding author, E-mail: jzhao@sio.org.cn

et al., 2014; Raiswell et al., 2018). Collectively, these factors facilitate the rapid proliferation of phytoplankton, which enhances the sequestration of carbon via the biological carbon pump, transferring organic carbon fixed through photosynthesis from the euphotic zone to the deep ocean (Volk and Hoffert, 1985; Boyd et al., 2019). The SIZ of the Southern Ocean contributes about 30% of the absorption of anthropogenic CO_2 and plays an important role in regulating the Earth's climate (Sallée et al., 2012; Delille et al., 2014; Frölicher et al., 2015; Meredith et al., 2019).

The annual formation and decay of seasonal sea ice represent the most significant seasonal physical phenomenon in the Southern Ocean, driving the spring bloom of phytoplankton and influencing the subsequent responses of higher trophic levels throughout the summer. The timing of sea ice melting earlier/later, can extend/shorten the growing season of phytoplankton, thereby enhancing/limiting primary production in the SIZ (Quéguiner, 2013). Concurrently, the reproductive cycles of many zooplankton species are synchronized with the phytoplankton growth season; variations in timing of ice melting may affect their reproductive timing and success rates (Rembauville et al., 2015), subsequently altering the structure of the biological pump and ultimately affecting its efficiency (Massom and Stammerjohn, 2010; Ardyna and Arrigo, 2020). The specific mechanisms underlying these dynamic processes remain not fully understood, which constrains our comprehension on the role of Antarctic marine ecosystem in climate change and carbon sequestration.

Sediment traps can collect samples of particulate matter settling at a specific depth in the water column over a set time interval, making them an ideal tool for studying the response mechanisms of the biological pump in the SIZ under varying sea ice melting conditions (Honjo et al., 2008). Research on sediment particles primarily focuses on total mass flux (TMF) and its components, including particulate organic carbon (POC), biogenic silica (BSi), particulate inorganic carbon (PIC), and lithogenic particle (Litho) fluxes, with POC and BSi being the predominant constituents (Honjo et al., 2008). The concentration and flux of POC represents a portion of primary production and is also the most closely monitored component (Salter et al., 2012; Rembauville et al., 2016). POC is complex in composition, primarily consisting of carbon contained in phytoplankton debris and spores, zooplankton carcasses, molts, and fecal matter (Rembauville et al., 2015; Manno et al., 2020; Trinh et al., 2023). BSi predominantly originates from the siliceous cell walls of plankton, particularly diatoms (over 90%), as well as radiolarians and silicoflagellates (DeMaster, 1981). In polar marine ecosystems, BSi is considered a vital ballast material, forming aggregates with phytoplankton debris and zooplankton feces, and which enhancing carbon sedimentation efficiency (Francois et al., 2002; Klaas and Archer, 2002; Wilson et al., 2012). Stable carbon and nitrogen isotopes ($\delta^{13}C$ and $\delta^{15}N$) are classic tools for tracing the sources of POC (Hwang et al., 2004, 2005; Mayer, 1994). Variations in the pathways and carbon sources utilized by different phytoplankton populations result in significant differences in their $\delta^{13}C$ values. For instance, carbon isotope signatures of sea ice diatoms exhibit distinct enrichment of ^{13}C, reaching values up to –8‰ (Dieckmann and Hellmer, 2003), whereas centric diatoms typically exhibited negative values around –30‰, and pennate diatoms around –21‰ (Lee et al., 2012; Zhang et al., 2023). In contrast, the feeding of zooplankton on phytoplankton only causes a minor fractionation, an average enrichment of 0.4‰ to 1‰ per trophic level (Peterson and Fry, 1987). Consequently, in shorter food chains, the $\delta^{13}C$ of POC is often utilized to reflect the succession of phytoplankton communities (Kopczyńska et al., 1995; Post, 2002). Fecal matter produced by zooplankton after ingesting phytoplankton is relatively enriched in ^{14}N, resulting in $\delta^{15}N$ values in zooplankton that are higher than those in phytoplankton. These values increase significantly with each trophic level with each trophic level, typically enriching 3‰ to 5‰ per trophic level, thereby serving as an excellent indicator of zooplankton contributions and community succession (Deniro and Epstein, 1981; Neill and Cornwell, 1992; Post, 2002).

Prydz Bay is a typical SIZ, which contains the third largest polynya in Antarctica—the Prydz Bay Polynya. Its annual average net primary productivity is (88.3 ± 19.4) g/(m^2·a) (in terms of C), second only to the Amundsen Sea Polynya and the Ross Ice Shelf Polynya (Arrigo and van Dijken, 2003), making it an important CO_2 sink in Antarctica (Arrigo and van Dijken, 2003; Arrigo et al., 2015). Prydz Bay exhibits significant variations in seasonal sea ice coverage. The ice-free period typically lasts from October to February, while the freezing period extends from March to September. The extent of sea ice reaches its maximum in September and its minimum in February (Zheng and Shi, 2011). During summer months, the community structure of phytoplankton and zooplankton in Prydz Bay rapidly responds to the melting of sea ice. At the onset of ice melt in austral spring (November), the initial bloom is comprised of ice algae, followed by a bloom of large centric diatoms as sea ice continues to retreat (Petrou et al., 2016). The dominant zooplankton during this period includes euphausiids and copepods, which exhibit relatively low grazing rates on phytoplankton (Skerratt et al., 1995; Guo et al., 2024). Once open water is established in austral summer, the dominant phytoplankton group shifts to pennate diatoms, eventually transitioning to mixotrophic cryptophytes (Kopczyńska et al., 1995; Taylor et al., 1997; Zhang et al., 2023). Meanwhile, euphausiids, large copepods, and small copepods increase significantly (Yang et al., 2013; Li and Yang, 2017; Pan et al., 2024). Sea ice diatoms and pennate diatoms are primarily responsible for the elevated $\delta^{13}C_{org}$ values, whereas *Phaeocystis*, naked flagellates, autotrophic dinoflagellates, and centric diatoms contributed to lower $\delta^{13}C_{org}$ val-

ues in particulate organic matter (Dieckmann and Hellmer, 2003; Kopczyńska et al., 1995). Consequently, the V-shaped $\delta^{13}C_{org}$ of POC effectively reflects the succession of algal community during summer (Han et al., 2018, 2019). Previous studies of particulate matter sedimentation in Prydz Bay have revealed significant inter-annual variability in TMF and its component fluxes, which are believed to be closely linked to differences in phytoplankton communities and the effects of ballasting (Han et al., 2018, 2019). However, it remains unclear whether these variations are related to the timing of sea ice melting. To address this question, this study analyzed sediment trap samples collected during the austral summers of 2019/2020 and 2020/2021 in Prydz Bay by the Chinese Antarctic Research Expedition. This study focused on the inter-annual variability in TMF and the component fluxes of particulate matter under conditions where the onset of sea ice melt differed by one and a half months, exploring the underlying reasons for these variations.

2 Methods and materials

2.1 *Study area and sampling*

Prydz Bay, located in Eastern Antarctica, is the third largest bay in Antarctica, following the Weddell Sea and Ross Sea. The circulation patterns within the Prydz Bay region are relatively simple, primarily involving the Antarctic Circumpolar Current (ACC), the Antarctic Slope Current (ASC) to the north, the Prydz Gyre (PG), and the Coastal Current of Antarctica (CoC) within the bay (Le et al., 1996; Shi et al., 2011). The eastern entrance of Prydz Bay is sheltered by the Four Ladies Bank and accumulations of icebergs, which limit the inflow of wind and wave energy into the bay, resulting in restricted deep-water exchange with the open ocean. Additionally, the westward flow within the bay is obstructed by the Fram Bank on the western side of the entrance, further reducing deep water exchange (Vaz and Lennon, 1996; Williams et al., 2010). Seasonal variations in Prydz Bay are marked by significant changes in sea ice, with complete freezing occurring across the continental shelf during austral winter, extending to approximately 57°S. In the austral summer, sea ice retreats southward, creating areas of ice-free open water within the inner bay. Sea ice originating from the Amery Ice Shelf (AIS) and West Ice Shelf predominantly grounds at Four Ladies Bank and Fram Bank, with concentrations ranging from 60% to 100%, notably lower at the AIS margin compared to regions north of 68°S (Roden et al., 2013, 2016). In the northern section of the bay's continental shelf, the presence of icebergs and sea ice restricts the propagation of wind and waves, thereby enhancing water stability (Roden et al., 2016). Consequently, Prydz Bay functions as a relatively enclosed system with high water stability, promoting the growth and proliferation of phytoplankton.

During the austral summer of 2019/2020 and 2020/2021, sediment traps (PARFLUX Mark78H-21, McLane, Inc., USA) were deployed in the Prydz Bay ice marginal zone to collect a time series of settling particulate samples. The trap stations were located at MP10(36/38) (2019/2020, 68.35°S, 75.11°E, water depth 579 m, trap depth 415 m) and MP10(37/39) (2020/2021, 68.28°S, 75.33°E, water depth 566 m, trap depth 405 m) (Fig. 1, Table 1). Each sediment trap had a collection area of 0.5 m² and sample bottles with a volume of 500 mL. To mitigate organic degradation caused by microbial activity, the sample bottles were filled with pre-filtered seawater con-

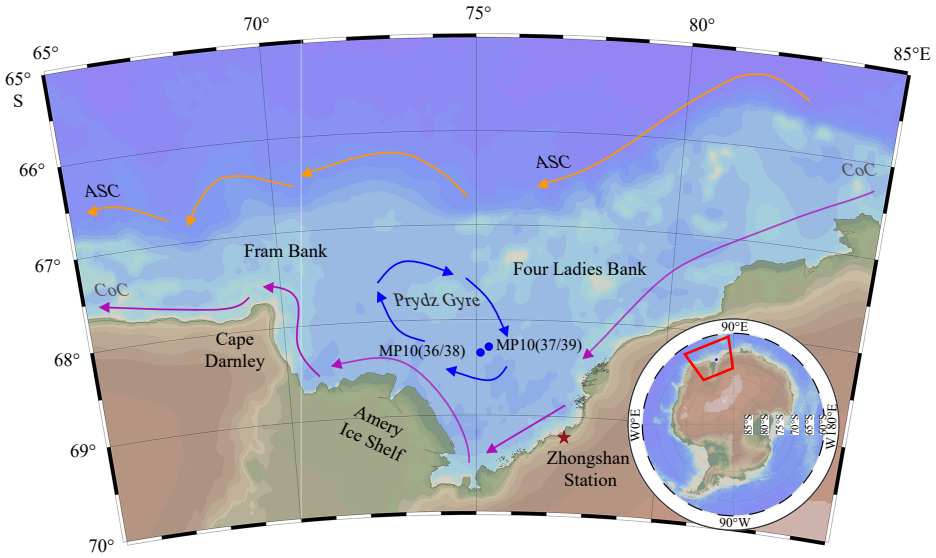


Fig. 1. Location of sediment trap sites MP10(36/38) (2019/2020) and MP10(37/39) (2020/2021) in Prydz Bay. The orange line with arrow is the Antarctic Slope Current (ASC); the blue lines with arrows denote Prydz Gyre (PG); the purple line with arrow is Antarctic Coastal Current (CoC). The red star is the location of the Chinese Antarctic Zhongshan Station.

tained formaldehyde (5%, *v*/*v*). The deployment of the sediment trap in 2020/2021 was delayed by approximately one month compared to the previous year due to sea ice coverage. Detailed information of sampling times and intervals is provided in Table 1.

2.2 *Laboratory analysis*

2.2.1 *Bulk analysis of sediment trap samples*

The collected samples were preserved at 4℃ and subsequently sieved through 1 mm Nylon mesh to remove swimmers. The particulate matter less than 1 mm was split into 10 equal aliquots using a rotary precision wet sample divider (McLane, Inc.). The samples were filtered through a pre-weighed 0.7 μm Millipore polycarbonate membrane, followed by washing the filtrate with ultrapure water to remove the salt, and were freeze-dried. TMF was calculated based on the dry weight of the sample. For the determine of carbon and nitrogen content, a portion of each sample was filtered on a 0.7 μm GF/F glass fiber filter, which had been previously combusted at 450℃ for 4 h and weighed. For POC analysis, samples were exposed to acid fumes for 12 h to remove the inorganic carbon, after which they were washed with ultra-pure water and dried at 50℃. The carbon and nitrogen concentrations were measured by a Euro Vector EA 3000 element analyzer. During the analytical procedure, a soil reference material (GSS-4) was interspersed at every sixth sample interval to serve as a quality control check, and the 1 σ precision of replicate analysis is +0.05% for carbon and nitrogen analysis. Every sample was measured twice, and the mean of two measurements is reported here. Particulate organic nitrogen (PON) was equal to total particulate nitrogen. Total carbon was measured directly, and PIC was calculated as the difference between the total carbon and POC. BSi concentrations were determined spectrophotometrically after digestion with sodium hydroxide, following the method described by Brzezinski and Nelson (1989), using certified reference material GBW08645. After microwave-assisted digestion, concentrations of total aluminum (Al) and iron (Fe) were determined by iNductively Coupled Plasma Optical Emission Spectroscopy (ICP-OES) (Thermo iCAP 7200). High purity ICP Multi Element Standard Solution XXI CertiPUR was utilized to create the calibration curve in the quantitative analysis. The contents of particulate organic matter (POM), calcium carbonate ($CaCO_3$), opal ($SiO_2 \cdot 0.4H_2O$) and lithogenic content (Litho) were calculated as POC (wt%) × 2.50, PIC (wt%) × 8.33, BSi (wt%) × 2.40 and Al (wt%) × 12.15, respectively (Thunell, 1998; Honjo et al., 2000; Kim et al., 2015; Han et al., 2019).

2.2.2 *$\delta^{15}N$ and $\delta^{13}C$ analyses of POM*

Two 1/10 aliquots of particulate material were prepared and analyzed for $\delta^{15}N$ and $\delta^{13}C$ following the methods described by Han et al. (2018). Isotope analyses were conducted using a Thermo Delta V advantage isotopic ratio mass spectrometer (IRMS) coupled to a Thermo Fisher FLASH2000 elemental analyzer. Caffeine and urea with known $\delta^{13}C$ and $\delta^{15}N$ values were used to monitor the measurement, respectively. Two parallel analyses were conducted for a part of samples and the precision of the replicate of $\delta^{13}C$ and $\delta^{15}N$ analysis is within the range of ±0.2‰.

2.2.3 *Remote sensing of sea ice concentration and chlorophyll a*

Sea ice concentration (SIC) data is sourced from the University of Bremen in Germany, with a spatial resolution of 3.125 km by 3.125 km and a temporal resolution of 1 d. Data within a 30 km by 30 km area centered on the observation station is selected for mean value calculation.

Remote sensing chlorophyll *a* (Chl *a*) concentration data is accessed from NASA Ocean Color website (https://oceancolor.gsfc.nasa.gov/l3/), which is selected from the Aqua-MODIS product with a spatial resolution of 4.0 km by 4.0 km and a temporal resolution of 1 d. Data within a 60 km by 60 km area centered on the observation station

Table 1. Biogeochemical parameters of sinking particles in Prydz Bay during austral summers of 2019/2020 and 2020/2021

CHINARE (year)	Cup	Start date	Duration/d	Flux/(mg·m^{-2}·d^{-1})							Molar ratio of BSi/POC	Content/%				$\delta^{13}C_{org}$/‰	$\delta^{15}N$/‰
				TMF	POC	PON	PIC	BSi	Fe	Al		Opal	POM	Litho	$CaCO_3$		
CHINARE-36 (2019/2020)	#1	2019.12.06	12	785.04	79.97	10.08	1.99	207.29	2.34	3.02	1.11	66.3	26.6	4.9	2.2	–25.4	1.8
	#2	2019.12.18	14	386.52	50.76	5.82	3.93	76.65	1.58	2.02	0.65	50.0	34.5	6.7	8.9	–27.6	2.1
	#3	2020.01.01	10	55.06	5.90	0.84	0.40	11.72	0.32	0.36	0.85	55.6	29.2	8.5	6.7	–26.9	3.4
	#4	2020.01.11	10	226.00	25.11	3.63	0.79	47.81	1.47	1.93	0.82	55.3	30.2	11.3	3.2	–28.7	3.5
	#5	2020.01.21	11	401.05	41.43	5.96	5.54	96.31	1.45	1.93	1.00	57.2	25.6	5.8	11.4	–29.7	3.0
	#6	2020.02.01	10	683.78	59.90	8.33	6.01	154.45	2.09	2.90	1.11	61.2	24.7	5.8	8.3	–28.8	2.2
	#7	2020.02.11	10	84.73	5.82	0.80	0.74	22.76	0.27	0.36	1.68	68.6	18.3	5.4	7.8	–28.0	3.0
CHINARE-37 (2020/2021)	#1′	2021.01.01	9	108.44	12.77	1.40	0.96	25.86	0.61	0.83	0.87	55.4	28.5	9.0	7.2	–30.6	1.0
	#2′	2021.01.10	10	598.15	59.71	6.40	1.00	151.53	1.38	1.88	1.09	66.8	27.4	4.2	1.5	–30.5	0.9
	#3′	2021.01.20	11	1 021.02	81.20	9.61	5.96	275.62	1.89	2.60	1.45	70.0	21.5	3.3	5.3	–29.9	0.8
	#4′	2021.01.31	10	1 491.70	99.46	12.68	3.00	448.20	1.61	2.18	1.93	78.2	18.1	1.9	1.8	–29.0	1.3
	#5′	2021.02.10	10	1 268.65	71.23	9.03	3.80	359.51	1.51	2.17	2.16	78.5	16.2	2.4	2.9	–27.8	1.5
	#6′	2021.02.20	14	548.27	28.77	3.96	1.57	185.16	1.25	1.74	2.76	80.7	13.1	3.8	2.4	–27.5	1.6

is selected for mean value calculation. Here, the data is presented as an 8-d average which were provided by the website.

3 Results

3.1 *Temporal variation of SIC and Chl a concentration*

During the austral summer of 2019/2020, the melting of sea ice proceeded similarly to previous years, with significant ice melt observed by late November. However, an anomalous increase in SIC was noted in January, lasting for over 20 d, during which ice concentrations peaked at 90% (Fig. 2a). In contrast, during the austral summer of 2020/2021, sea ice retreated about one and a half months later than in austral summer of 2019/2020, with some ice still present in early January (Fig. 2a). This duration and extent were notably less than the previous year, despite no significant change in the onset of freezing.

Satellite-derived Chl *a* concentrations were constrained by SIC, becoming available only after the onset of sea ice melting. In the austral summer of 2019/2020, Chl *a* concentration exhibited four distinct peaks: Peak Ⅰ occurred in middle to late November, which was predicted trend based on previous observations and research (Han et al., 2018, 2019), showing partial decline with a peak value of no less than 1.2 mg/m^3; Peak Ⅱ was observed at the end of December with a value of 1.5 mg/m^3; Peak Ⅲ occurred in mid-February with a value of 3.7 mg/m^3; Peak Ⅳ was recorded in early March, achieving a maximum of 4.0 mg/m^3, rapidly declining to 1.0 mg/m^3 within a week post-peak (Fig. 2a). In contrast, during the austral summer of 2020/2021, two Chl *a* concentration peak revealed two peaks of Chl *a* concentration: Peak Ⅴ was observed in mid-February with a value of 1.2 mg/m^3; a more prominent Peak Ⅵ occurred in late February, reaching a maximum of 3.0 mg/m^3, which subsequently decreased to 0.3 mg/m^3 within a week post-peak (Fig. 2a). The timing of Peaks Ⅴ and Ⅵ occurred one week earlier than that of Peaks Ⅲ and Ⅳ, respectively.

3.2 *Mass and elemental fluxes*

In the austral summer of 2019/2020, TMF value ranged within 55.06–785.04 mg/(m^2·d), with an average of 386.22 mg/(m^2·d) (Table 1). Two notable peaks occurred in mid-December 2019 and early-February 2020, reaching 785.04 mg/(m^2·d) and 683.78 mg/(m^2·d), respectively (Fig. 2b). In contrast, during the austral summer of 2020/2021, TMF values were higher, ranging within 108.44–1 491.70 mg/(m^2·d), with an average of 853.44 mg/(m^2·d) (Table 1).

During the former austral summer, the flux of BSi ranged within 11.72–207.29 mg/(m^2·d), averaging 88.14 mg/(m^2·d), while in the latter austral summer, BSi fluxes varied from 25.86 mg/(m^2·d) to 448.20 mg/(m^2·d), averaging 240.98 mg/(m^2·d) (Table 1, Fig. 2b).

During the former austral summer, POC flux ranged within 5.82–79.97 mg/(m^2·d), averaging 40.17 mg/(m^2·d), while PON flux ranged within 0.80–10.08 mg/(m^2·d), averaging 5.25 mg/(m^2·d) (Table 1, Figs 2c and d). In the latter austral summer, POC flux varied within 12.77–99.46 mg/(m^2·d), averaging 58.04 mg/(m^2·d), while PON flux ranged from 1.40 mg/(m^2·d) to 12.68 mg/(m^2·d), averaging 7.11 mg/(m^2·d) (Table 1, Figs 2c and d). Unlike TMF and BSi fluxes, the peak values of POC and PON fluxes did not significantly differ between the two summers (Table 1, Figs 2c and d).

For the former austral summer, Al flux ranged from 0.36 mg/(m^2·d) to 3.02 mg/(m^2·d), averaging 1.84 mg/(m^2·d), and Fe flux ranged from 0.27 mg/(m^2·d) to 2.34 mg/(m^2·d), averaging 1.40 mg/(m^2·d), with peak values coinciding with POC and BSi peaks (Table 1, Fig. 2e). In the latter austral summer, Al flux varied from 0.83 mg/(m^2·d) to 2.60 mg/(m^2·d), averaging 1.92 mg/(m^2·d), and Fe flux ranged from 0.61 mg/(m^2·d) to 1.89 mg/(m^2·d), averaging 1.39 mg/(m^2·d) (Table 1, Fig. 2e).

For the former summer, the flux of PIC ranged within 0.40–6.01 mg/(m^2·d), averaging 2.85 mg/(m^2·d), with peak values occurring in mid-to-late December (Table 1). In the latter austral summer, PIC flux varied within 0.96–5.96 mg/(m^2·d), averaging 2.72 mg/(m^2·d), with the highest values observed in late January (Table 1).

3.3 *Molar ratios*

The molar ratio of BSi/POC ranged from 0.65 to 1.68 with an average of 1.14 during the former austral summer; and ranged from 0.87 to 2.76 with an average of 1.85 during the latter summer (Table 1, Fig. 2b). The molar ratio of BSi/POC exhibited a minor initial decline followed by a gradual increase in the former austral summer, maintaining a stable value throughout January with minimal fluctuations (Fig. 2b). In contrast, the latter austral summer saw a consistent and gradual increase in this ratio over time (Fig. 2b).

3.4 *Particulate stable isotope data*

The $\delta^{13}C_{org}$ values from traps during the previous austral summer ranged from –29.7‰ to –25.4‰, with an average of –27.9‰ (Table 1 , Table A1, and Fig. 2c). From December 2019 to late-January 2020, the value of $\delta^{13}C_{org}$ exhibited a general downward trend from Cup #1 to Cup #5, with a slight increase in Cup #3, indicating a more negative trend. From late-January to mid-February 2020, the value of $\delta^{13}C_{org}$ progressively increased from Cup #4 to Cup #7, though the magnitude of this increase was significantly smaller than the previous decrease. In contrast, during the subsequent austral summer, the value of $\delta^{13}C_{org}$ from traps ranged from –30.6‰ to –27.5‰, with an aver-

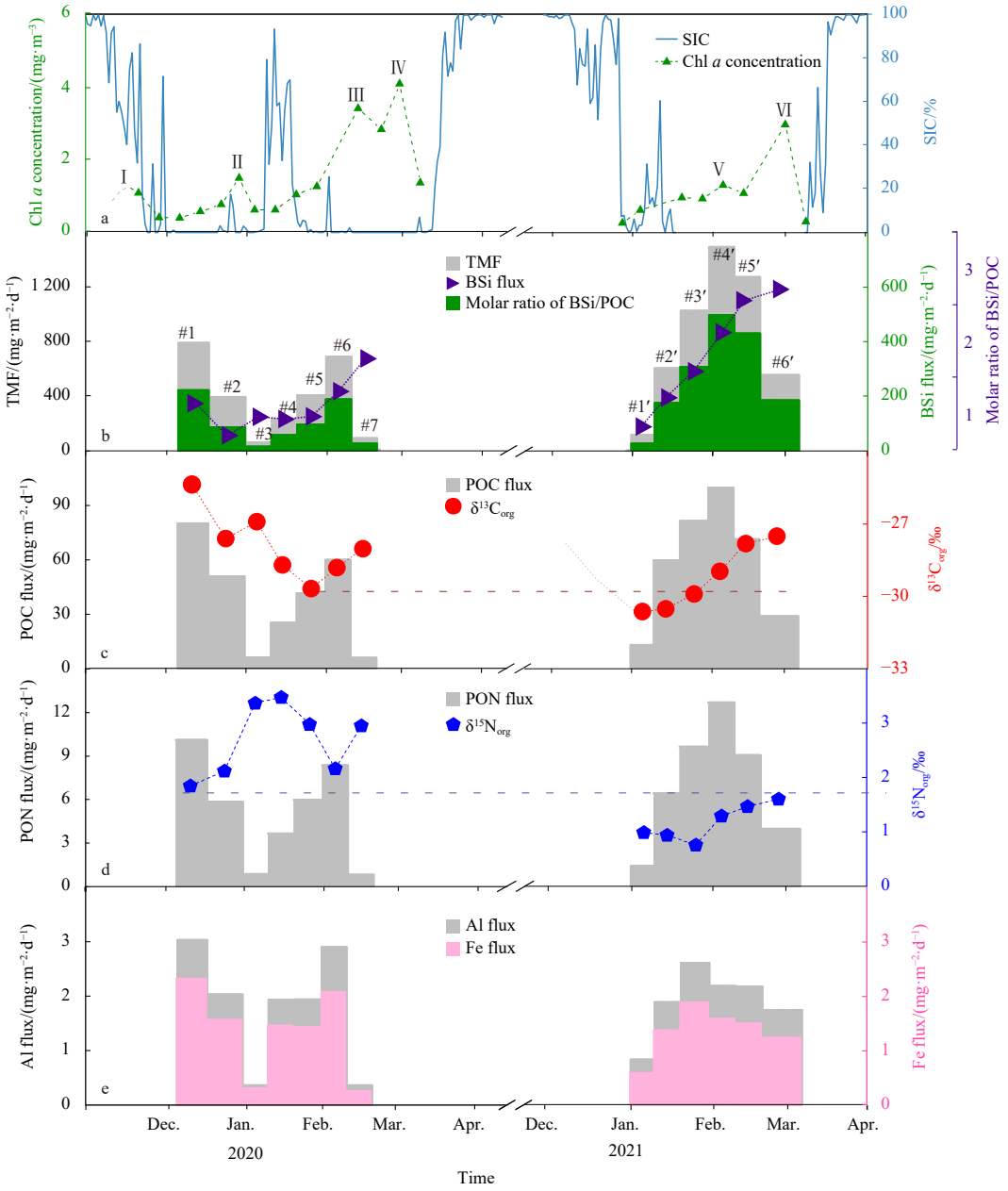


Fig. 2. Time-series fluxes of various components in Prydz Bay during austral summer of 2019/2020 and 2020/2021. Chl *a*: remote sensing chlorophyll *a*; SIC: sea ice concentration; TMF: total mass flux; POC: particulate organic carbon; PON: particulate organic nitrogen; BSi: biogenic silica; $\delta^{13}C_{org}$: organic stable carbon isotopic composition; $\delta^{15}N$: organic stable nitrogen isotopic composition; Al: aluminum; Fe: iron. Ⅰ–Ⅵ are Chl *a* peaks; #1–#7 represent the cup number of the first summer; #1′–#6′ represent the cup number of the second summer.

age of –29.2‰ (Table 1, Fig. 2c). Throughout this period, the value of $\delta^{13}C_{org}$ consistently showed a gradual upward trend, suggesting a shift towards less negative values. The $\delta^{15}N$ data from traps of the former austral summer ranged from 1.6‰ to 3.5‰ with an average of 2.7‰ (Table 1, Fig. 2d). From December 2019 to January 2020, values gradually became positive, then fluctuated, showing a noticeable positive trend in the final trap. The $\delta^{15}N$ data from traps of the latter austral summer ranged from 0.8‰ to 1.6‰ with an average of 1.2‰ (Table 1, Fig. 2d). Throughout January of the latter austral summer, values showed a slight gradual decrease, followed by a trend towards further negative values. Overall, $\delta^{15}N$ values in the latter summer were significantly lower compared to the former austral summer.

3.5 *Geochemical composition of particulate matter*

The settling particulate matter collected in sediment traps can be categorized into biogenic and lithogenic fluxes. Biogenic fluxes include opal, POM, and $CaCO_3$. Opal primarily consists of diatom shells, with a chemical for-

mula of $SiO_2 \cdot 4H_2O$. During the former austral summer, opal represented 50.0% to 68.6% of the total weight, while in the latter summer, it varied from 55.4% to 80.7% (Fig. 3). POM flux contribution to TMF was around 18.3% to 34.5% in the former austral summer and 13.1% to 28.5% in the latter summer (Table 1, Fig. 3). $CaCO_3$ represented 2.2% to 11.4% of the total material flux in the former austral summer, while in the latter summer, it ranged from 1.5% to 7.2%. The flux of Litho contribution to the TMF was 4.9% to 11.3% in the former austral summer and 1.9% to 9.0% in the latter austral summer (Table 1, Fig. 3).

Correlations between TMF and each of the flux components of both austral summers are shown in Fig. 4. Among them, an obvious positive correlations exist between opal and POM fluxes ($r^2 = 0.950$, $p < 0.01$ for the austral summer of 2019/2020; $r^2 = 0.898$, $p < 0.05$ for the austral summer of 2020/2021), and both are strongly correlated with TMF in both summers (Fig. 4).

4 Discussion

4.1 *Annual variations in summer particle flux dynamics*

Along the Antarctic ice edge, the seasonal melting of sea ice during austral spring and summer correlates closely with the blooming of diatoms and the export of sedimentary particles (Nelson and Smith, 1986). In Prydz Bay, increases in TMF and POC fluxes appear to commence immediately following the complete disappearance of sea ice, typically with minimal lag, often within just a few weeks (Han et al., 2018; Yu et al., 2023). The response patterns of Chl *a* concentration, TMF, POM flux, and BSi flux between these two summers highlighted significant differences, with TMF, POM, and BSi showing higher correlations (Fig. 4), underscoring the critical role of diatom blooms in their output.

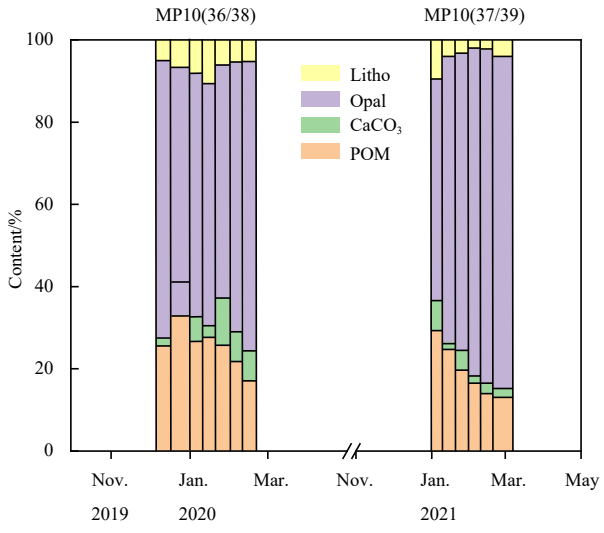


Fig. 3. Geochemical composition of particulate samples over time with the four major components normalized to 100%.

During the austral summer of 2019/2020, satellite data of Chl *a* concentration revealed a decline during the latter stages of bloom Peak Ⅰ (Fig. 2a), which corresponded with similarly to observations of first peak of TMF, BSi and POC fluxes collected in mid-December from Cup #1 (Figs 2b and c), consistent with flux values reported by Han et al. (2019). From mid-December to early January, Chl *a* concentration increased significantly, paralleling the gradual decrease in TMF, BSi and POC fluxes from Cup #1 to Cup #3, which indicated an increasing productivity but a low export of particle fluxes from upper water. At Peak Ⅰ of Chl *a* concentration, Cup #1 recorded a $\delta^{13}C_{org}$ value of –25.4‰, representing the middle to late phase following the complete melting of sea ice, reflecting a combined contribution of sea ice diatoms and centric diatoms to POC (Dieckmann and Hellmer, 2003). The retreat of sea ice diatoms due to complete sea ice melt led to an increased dominance of centric diatoms within the diatom community (Lin et al., 2021). Despite the declining trends in TMF, BSi and POC fluxes from Cup #1 to Cup #3, Chl *a* concentration value experienced Peak Ⅱ, likely be linked to the bloom of *Phaeocystis* sp. in late December in study area (Kopczyńska et al., 1995). Due to inefficient sinking of *Phaeocystis* sp. despite high productivity, it was less to reach depths below the euphotic zone (Reigstad and Wassmann, 2007). The $\delta^{13}C_{org}$ value of Cup #3 shifted positively compared to Cup #2 (Fig. 2c), likely influenced by increased sea ice algae inputs in late December, when SIC significantly increased (Fig. 2a). Sea ice diatoms are located at the bottom of the ice. As the sea ice melts, they enter the underlying water, making their presence more noticeable in the early stages of ice melting (Arrigo et al., 2015). So, at the end of December 2019, there would be an input of sea ice diatoms in Cup #3, leading to an increase in $\delta^{13}C_{org}$ value. Then, in mid-January 2020, which was the height of austral summer, the sea ice diatoms at the bottom of the sea ice have already been released, and the aggregation of sea ice could not bring in the input of sea ice diatoms. The low BSi flux in Cup #3 representd a reduction in the overall productivity of diatoms. The input from sea ice diatoms brought in by sea ice, was small, thus has a limited impact on the overall enhancement of diatom productivity. However, sea ice diatoms have extremely high $\delta^{13}C$-rich value, and an increase in their relative proportion within the overall diatom community could easily lead to an increase in the $\delta^{13}C_{org}$ values of POM. From Cup #3 to Cup #7, BSi flux gradually increased, with $\delta^{13}C_{org}$ values shifting gradually from –26.9‰ to –29.7‰, then to –28.0‰, reflecting the transition from *Phaeocystis* sp. to centric diatom-dominated, then to pennate diatom-dominated communities (Kopczyńska et al., 1995). Notably, the second flux peak of TMF, BSi, and POC fluxes in Cup #6 occurred prior to the Chl *a* concentration Peaks Ⅲ and Ⅳ. In con-

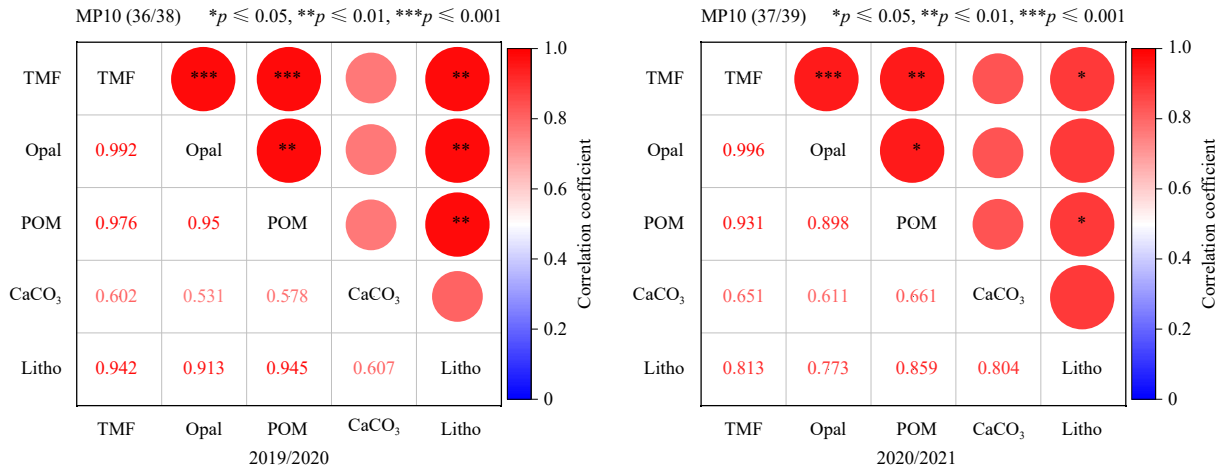


Fig. 4. Correlation coefficients between fluxes of different major components in the sediment trap samples ($^{***}p \leqslant 0.001$, $^{**}p \leqslant 0.01$, $^{*}p \leqslant 0.05$).

trast, TMF, BSi, and POC fluxes of Cup #7 suddenly decreased while Chl *a* concentration reached at Peaks Ⅲ and Ⅳ, indicating the productivity of the total diatom community decreased drastically, and the high Chl *a* concentration value related to non-diatom species such as flagellates and autotrophic dinoflagellates at this time, which had been reported previously (Kopczyńska et al., 1995; Taylor et al., 1997). The gradual increase in $\delta^{13}C_{org}$ values observed in Cups #4–#7 primarily reflected the increasing proportion of pennate diatoms within the diatom community. As these smaller-sized algae, coupled with reduced diatom populations, had significantly lower sedimentation rate and easily mineralized in the surface water, resulting in a limited contribution of the entire algal community to POC flux (Arrigo and Thomas, 2004). This aligns with the observation: POC and BSi fluxes were highly correlated in summer (Fig. 4), suggesting diatoms as the main source of settling organic matter.

During the austral summer of 2020/2021, sediment traps deployed after complete sea ice melt, which approximately one and a half months later than in 2019/2020. Following the sea ice melt, Chl *a* concentration values gradually increased, with pronounced Chl *a* concentration peaks observed throughout the summer, specifically Peaks Ⅴ and Ⅵ in February and March, respectively; Peak Ⅵ exhibited higher values than Peak Ⅴ. The $\delta^{13}C_{org}$ values shifted from –30.6‰ to –27.5‰, reflecting the succession from centric diatoms to pennate diatoms within the diatom community (Kopczyńska et al., 1995). From late December to early February, Chl *a* concentration level gradually increased to Peak Ⅴ, accompanied by rapid increases in TMF and BSi, indicating a promoted of pennate diatom productivity. Unlike Cups #3 and #4 of the summer of 2019/2020, Cups #1′ and #2′ exhibited $\delta^{13}C_{org}$ values prominently skewed towards –30.0‰ in the first half of January, suggesting centric diatoms dominated the community post-complete sea ice melt. From late February to early March, Cups #4′ to #6′ recorded gradual declines in TMF, BSi, and POC fluxes, while Chl *a* concentration peaked at the end of February, similarly to the late stage of 2019/2020, with the primary algal bloom during Peak Ⅵ likely dominated by non-diatom algae.

Comparing these two summers reveals that sea ice plays a vital role in the succession of algae communities, the ^{13}C-depleted of POC in 2020/2021 summer indicated that delayed sea ice melt may promote the relative productivity of centric diatoms to the overall algal community due to disappearance of *Phaeocystis* sp. bloom. The values of Chl *a* concentration were similar within January to March between these two summers, however TMF, BSi, and POC fluxes in 2020/2021 summer much higher compared to 2019/2020 summer cannot be explained higher the relative productivity of centric diatoms alone. The insignificant increase in POC export, potentially attributable to changes in weakened efficiency of POM assimilated by zooplankton, which could be influenced by the delayed sea ice melt.

4.2 *Remineralization and export of POM influenced by sea ice melting time*

In Prydz Bay, high productivity is associated with rapid remineralization of organic carbon within the water column. Summer data indicate that the concentration of POC drops swiftly from 482.9 μg/L at the surface to 42.4 μg/L in the mixed layer at a depth of 200 m, reflecting that most of POM at the surface is transformed into dissolved organic carbon and dissolved inorganic carbon, indicating a low efficiency of vertical carbon export (Jiang et al., 2024). This phenomenon implicates complex biogeochemical cycling mechanisms, including zooplankton consumption and excretion (Lampitt et al., 1993; Boyd et al., 2019), zooplankton vertical migration (Boyd et al., 2019), particle aggregation and fragmentation (Briggs et al., 2020), and degradation by marine bacteria (Giering et al., 2014). Those factors all significantly influence the fluxes of silicon and carbon, thereby affecting the variability of BSi/POC observed in the samples collected by the two sets of sediment traps.

In the Southern Ocean, a high BSi/POC ratio is usually related to the three primary factors. First, the lateral transport of resuspended sediments may increase the BSi/POC values in the samples of the sediment trap (Collier et al., 2000). Considering minimal differences in the location and depth of sediment trap deployment over two years, the interannual difference in BSi/POC due to sediment resuspension may be limited. Second, Fe limitation is a significant factor contributing to the increase in the BSi/POC ratio of diatoms. Under non-limiting conditions, the typical BSi/POC ratio of well-nourished diatoms is 0.13, but under iron-limited conditions, this ratio can increase by 2 times to 3 times or more (Hutchins and Bruland, 1998; Takeda, 1998). During the austral summer, the BSi/POC ratios in Prydz Bay show a consistent pattern (Han et al., 2018, 2019), increasing gradually from December to March. This period sees high productivity in the SIZ, where diatom blooms deplete available iron, particularly the bioavailable form crucial for diatoms. This iron scarcity may elevate diatom Si/C uptake ratios, a response to iron stress as indicated by Brzezinski and Nelson (1989). Notably, during the two summers, the flux of Fe was relatively consistent (Fig. 2e). Therefore, while Fe limitation may be present, it does not appear to be the primary determinant of the differences of BSi/POC ratio between these two summers. Third, grazing and aggregation of diatom lead to decoupling of organic carbon and BSi degradation, resulting in variation of BSi/POC ratio (Pondaven et al., 2007). Meanwhile, the culture experiment showed when diatoms are exposed to grazers, the BSi/POC ratio could increase by a factor of 2–3 (Pondaven et al., 2000, 2007). So, there are two possible explanations to the differences of BSi/POC ratio between these two summers: (1) a promotion of BSi decomposition in the former summer relative to the latter summer; (2) high stress from grazers increasing diatoms' synthesis of BSi in latter summer relative to the former summer.

The delayed melting of sea ice can influence the timing of algal blooms, which subsequently affects the activity of zooplankton such as krill (Moline et al., 2008; Schmidt et al., 2014). During the austral summer of 2019/2020, a substantial quantity of krill molt and individuals were collected in the sediment traps (Fig. 5a), indicating relatively high biological activity in the study area at that time. Conversely, in the austral summer of 2020/2021, the number of krill molt and individuals captured in the traps significantly decreased (Fig. 5b), suggesting potential seasonal variations in biological activity or alterations in ecosystem structure. Furthermore, the $\delta^{15}N$ values in particulate matter from these two summers reflect the processing of organic matter by consumers, including krill (Lourey et al., 2003). Two factors influencing $\delta^{15}N$ in particulate matter are as follows. First, the proliferation of phytoplankton leads to substantial consumption of nitrate in the water column, resulting in the enhanced uptake of enriched $\delta^{15}N$ (Altabet and Francois, 2001). Second, secondary processes occurring in the upper and mid-water column, such as trophic transfer, particle reworking, and mid-water remineralization, can substantially elevate $\delta^{15}N$ values in sinking particulate material (Altabet and Francois, 2001; Lourey et al., 2003). The upper water in the study area contains high concentrations of nitrate (30–40 μmol/L) that remains are largely unutilized by phytoplankton, even during periods of phytoplankton growth (Sigman et al., 1999; DiFiore et al., 2006). Therefore, nitrate does not a limiting factor for biological productivity in study area. Consequently, the elevated $\delta^{15}N$ values in particulate matter from these two sets of traps are unlikely to be associated with excessive nitrate consumption due to phytoplankton blooms. Instead, they are more likely influenced by trophic transfer, particle reworking, or mid-water remineralization processes.

The $\delta^{15}N$ value and count of krill in Cups #1′–#6′ from the austral summer of 2020 and 2021 within January to March are significantly lower than those in the Cups #3–#7 from the previous summer with the same time (Figs 2d and 5), indicating less intense feeding activity during the former summer, which can be attributed to the adverse effects of a prolonged period of sea ice persistence (Williams et al., 2008). Moreover, the stress response of diatoms was observed under experimental conditions (Pondaven et al., 2007). In an open water body system

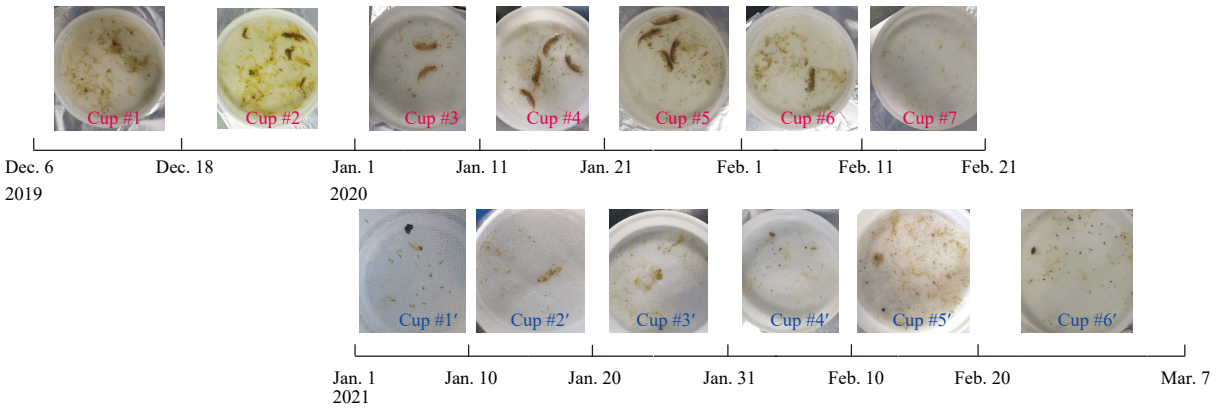


Fig. 5. Krill molt and individuals in the traps of 2019/2020 (Cups #1–#7) and 2020/2021 (Cups #1′–#6′) summer.

like Prdyz Bay, such stress should be significantly reduced, especially considering that the feeding intensity already decreased compared to the latter summer. So, stress response of diatoms by grazing should not be accounted for the higher value of BSi/POC of the summer of 2020/2021. The feeding activity of zooplankton can lead to the consume of organic carbon and the fragmentation of diatom frustules, thereby enhancing the dissolution rate of biogenic silica (Pondaven et al., 2007). Additionally, zooplankton enhance transport efficiency through their feces and vertical migration, which is conducive to the preservation of organic carbon (Dagg et al., 2003). Both factors leaded to a more slow-growing and lower BSi/POC ratio in the summer of 2019/2020 than that in the summer of 2020/2021. Therefore, when evaluating the impact of zooplankton on the biological pump, the promoted turnover rate of Si they facilitated should not be overlooked.

5 Summary and implications

Overall, the variation in retreat time of sea ice exerts a significant influence on the export of particulate matter in the Antarctic marginal sea. This phenomenon is closely linked to the succession of phytoplankton communities and the growth and grazing activities of zooplankton. The delayed sea ice retreat in the austral summer of 2020/2021 than 2019/2020 led to a promote of centric diatoms, weakened zooplankton grazing, potentially facilitated the efficient sinking of organic matter. These interconnected factors underscore the complex dynamics by which sea ice influences the productivity, community composition, and biogeochemical cycling within the polar marine ecosystem.

Acknowledgement

The authors wish to thank the CHINARE-36, 37, and 38 team members and the crew of R/V *Xuelong* and R/V *Xuelong 2* in the field work.

References

Altabet M A, Francois R. 2001. Nitrogen isotope biogeochemistry of the Antarctic Polar Frontal Zone at 170°W. Deep-Sea Research Part Ⅱ: Topical Studies in Oceanography, 48(19–20): 4247–4273, doi: 10.1016/S0967-0645(01)00088-1

Ardyna M, Arrigo K R. 2020. Phytoplankton dynamics in a changing Arctic Ocean. Nature Climate Change, 10(10): 892–903, doi: 10.1038/s41558-020-0905-y

Arrigo K R, Thomas D N. 2004. Large scale importance of sea ice biology in the Southern Ocean. Antarctic Science, 16(4): 471–486, doi: 10.1017/s0954102004002263

Arrigo K R, van Dijken G L. 2003. Phytoplankton dynamics within 37 Antarctic coastal polynya systems. Journal of Geophysical Research: Oceans, 108(C8): 3271, doi: 10.1029/2002JC001739

Arrigo K R, van Dijken G L, Strong A L. 2015. Environmental controls of marine productivity hot spots around Antarctica. Journal of Geophysical Research: Oceans, 120(8): 5545–5565, doi: 10.1002/2015jc010888

Boyd P W, Claustre H, Levy M, et al. 2019. Multi-faceted particle pumps drive carbon sequestration in the ocean. Nature, 568(7752): 327–335, doi: 10.1038/s41586-019-1098-2

Briggs N, Dall'Olmo G, Claustre H. 2020. Major role of particle fragmentation in regulating biological sequestration of CO_2 by the oceans. Science, 367(6479): 791–793, doi: 10.1126/science.aay1790

Brzezinski M A, Nelson D M. 1989. Seasonal changes in the silicon cycle within a Gulf Stream warm-core ring. Deep-Sea Research Part A. Oceanographic Research Papers, 36(7): 1009–1030, doi: 10.1016/0198-0149(89)90075-7

Collier R, Dymond J, Honjo S, et al. 2000. The vertical flux of biogenic and lithogenic material in the Ross Sea: moored sediment trap observations 1996–1998. Deep-Sea Research Part Ⅱ: Topical Studies in Oceanography, 47(15–16): 3491–3520, doi: 10.1016/S0967-0645(00)00076-X

Dagg M J, Urban-Rich J, Peterson J O. 2003. The potential contribution of fecal pellets from large copepods to the flux of biogenic silica and particulate organic carbon in the Antarctic Polar Front region near 170°W. Deep-Sea Research Part Ⅱ: Topical Studies in Oceanography, 50(3–4): 675–691, doi: 10.1016/S0967-0645(02)00590-8

Delille B, Vancoppenolle M, Geilfus N X, et al. 2014. Southern Ocean CO_2 sink: the contribution of the sea ice. Journal of Geophysical Research: Oceans, 119(9): 6340–6355, doi: 10.1002/2014JC009941

DeMaster D J. 1981. The supply and accumulation of silica in the marine environment. Geochimica et Cosmochimica Acta, 45(10): 1715–1732, doi: 10.1016/0016-7037(81)90006-5

Deniro M J, Epstein S. 1981. Influence of diet on the distribution of nitrogen isotopes in animals. Geochimica et Cosmochimica Acta, 45(3): 341–351, doi: 10.1016/0016-7037(81)90244-1

Dieckmann G S, Hellmer H H. 2003. The importance of sea ice: an overview. In: Thomas D N, Dieckmann G S, eds. Sea Ice: An Introduction to its Physics, Chemistry, Biology and Geology. London: Blackwell Science Ltd, 1–21, doi: 10.1002/9780470757161.ch1

DiFiore P J, Sigman D M, Trull T W, et al. 2006. Nitrogen isotope constraints on subantarctic biogeochemistry. Journal of Geophysical Research: Oceans, 111(C8): C08016, doi: 10.1029/2005JC003216

Francois R, Honjo S, Krishfield R, et al. 2002. Factors controlling the flux of organic carbon to the bathypelagic zone of the ocean. Global Biogeochemical Cycles, 16(4): 34-1–34-20, doi: 10.1029/2001GB001722

Frölicher T L, Sarmiento J L, Paynter D J, et al. 2015. Dominance of the Southern Ocean in anthropogenic carbon and heat uptake in CMIP5 models. Journal of Climate, 28(2): 862–886, doi: 10.1175/JCLI-D-14-00117.1

Giering S L C, Sanders R, Lampitt R S, et al. 2014. Reconciliation of the carbon budget in the ocean's twilight zone. Nature, 507(7493): 480–483, doi: 10.1038/nature13123

Guo Xiaoze, Zhao Jun, Pan Jianming, et al. 2024. Organic matter composition in sediments recording sea surface phytoplankton community structure in Prydz Bay of Antarctica. Organic Geochemistry, 195: 104828, doi: 10.1016/j.orggeochem.2024.104828

Han Zhengbing, Hu Chuanyu, Sun Weiping, et al. 2019. Characteristics of particle fluxes in the Prydz Bay polynya, Eastern Antarctica. Science China: Earth Sciences, 62(4): 657–670, doi: 10.1007/s11430-018-9285-6

Han Zhengbing, Sun Weiping, Fan Gaojing, et al., 2018. Sinking particle fluxes during austral summer in the Prydz Bay polynya, Antarctica. China Environmental Science (in Chinese), 38(5): 1923–1934, doi: 10.19674/j.cnki.issn1000-6923.2018.0218

Honjo S, Francois R, Manganini S, et al. 2000. Particle fluxes to the interior of the Southern Ocean in the Western Pacific sector along 170°W. Deep-Sea Research Part Ⅱ: Topical Studies in Oceanography, 47(15–16): 3521–3548, doi: 10.1016/S0967-0645(00)00077-1

Honjo S, Manganini S J, Krishfield R A, et al. 2008. Particulate organic carbon fluxes to the ocean interior and factors controlling the biological pump: a synthesis of global sediment trap programs since 1983. Progress in Oceanography, 76(3): 217–285, doi: 10.1016/j.pocean.2007.11.003

Hutchins D A, Bruland K W. 1998. Iron-limited diatom growth and Si:N uptake ratios in a coastal upwelling regime. Nature, 393(6685): 561–564, doi: 10.1038/31203

Hwang J, Druffel E R M, Griffin S, et al. 2004. Temporal variability of $\Delta^{14}C$, $\delta^{13}C$, and C/N in sinking particulate organic matter at a deep time series station in the Northeast Pacific Ocean. Global Biogeochemical Cycles, 18(4): GB4015, doi: 10.1029/2004GB002221

Hwang J, Druffel E R M, Komada T. 2005. Transport of organic carbon from the California coast to the slope region: a study of $\Delta^{14}C$ and $\delta^{13}C$ signatures of organic compound classes. Global Biogeochemical Cycles, 19(2): GB2018, doi: 10.1029/2004GB002422

Jiang Bin, Zhao Jun, Li Dong, et al. 2024. Molecular composition evolution of dissolved organic matter with water depth in Prydz Bay of East Antarctic: carbon export implications. Journal of Geophysical Research: Oceans, 129(7): e2023JC020571, doi: 10.1029/2023JC020571

Kim M, Hwang J, Kim H J, et al. 2015. Sinking particle flux in the sea ice zone of the Amundsen shelf, Antarctica. Deep-Sea Research Part Ⅰ: Oceanographic Research Papers, 101: 110–117, doi: 10.1016/j.dsr.2015.04.002

Klaas C, Archer D E. 2002. Association of sinking organic matter with various types of mineral ballast in the deep sea: implications for the rain ratio. Global Biogeochemical Cycles, 16(4): 63-1–63-14, doi: 10.1029/2001GB001765

Kopczyńska E E, Goeyens L, Semeneh M, et al. 1995. Phytoplankton composition and cell carbon distribution in Prydz Bay, Antarctica: relation to organic particulate matter and its $\delta^{13}C$ values. Journal of Plankton Research, 17(4): 685–707, doi: 10.1093/plankt/17.4.685

Lampitt R S, Hillier W R, Challenor P G. 1993. Seasonal and diel variation in the open ocean concentration of marine snow aggregates. Nature, 362(6422): 737–739, doi: 10.1038/362737a0

Lannuzel D, Schoemann V, de Jong J, et al. 2007. Distribution and biogeochemical behaviour of iron in the East Antarctic sea ice. Marine Chemistry, 106(1–2): 18–32, doi: 10.1016/j.marchem.2006.06.010

Le Kengtang, Shi Jiuxin, Yu Kangling. 1996. An analysis on water masses and thermohaline structures in the region of Prydz Bay, Antarctica. Oceanologia et Limnologia Sinica (in Chinese), 27(3): 236–244

Lee S H, Kim B K, Yun M S, et al. 2012. Spatial distribution of phytoplankton productivity in the Amundsen Sea, Antarctica. Polar Biology, 35(11): 1721–1733, doi: 10.1007/s00300-012-1220-5

Li Chaolun, Yang Guang. 2017. Progress of Chinese zooplankton ecology research in Prydz Bay, Antarctica. Advances in Polar Science, 28(2): 120–128, doi: 10.13679/j.advps.2017.2.00120

Lin Yajuan, Moreno C, Marchetti A, et al. 2021. Decline in plankton diversity and carbon flux with reduced sea ice extent along the western Antarctic Peninsula. Nature Communications, 12(1): 4948, doi: 10.1038/s41467-021-25235-w

Lourey M J, Trull T W, Sigman D M. 2003. Sensitivity of $\delta^{15}N$ of nitrate, surface suspended and deep sinking particulate nitrogen to seasonal nitrate depletion in the Southern Ocean. Global Biogeochemical Cycles, 17(3): 1081, doi: 10.1029/2002GB001973

Manno C, Fielding S, Stowasser G, et al. 2020. Continuous moulting by Antarctic krill drives major pulses of carbon export in the north Scotia Sea, Southern Ocean. Nature Communications, 11(1): 6051, doi: 10.1038/s41467-020-19956-7

Massom R A, Stammerjohn S E. 2010. Antarctic sea ice change and variability – Physical and ecological implications. Polar Science, 4(2): 149–186, doi: 10.1016/j.polar.2010.05.001

Mayer L M. 1994. Surface area control of organic carbon accumulation in continental shelf sediments. Geochimica et Cosmochimica Acta, 58(4): 1271–1284, doi: 10.1016/0016-7037(94)90381-6

Meredith M, Sommerkorn M, Cassotta S, et al. 2019. Polar regions. In: Pörtner H O, Roberts D C, Masson-Delmotte V, et al., eds. IPCC Special Report on the Ocean and Cryosphere in a Changing Climate. Cambridge: Cambridge University Press, 203–320

Moline M A, Karnovsky N J, Brown Z, et al. 2008. High latitude changes in ice dynamics and their impact on polar marine ecosystems. Annals of the New York Academy of Sciences, 1134: 267–319, doi: 10.1196/annals.1439.010

Neill C, Cornwell J C. 1992. Stable carbon, nitrogen, and sulfur isotopes in a prairie marsh food web. Wetlands, 12(3): 217–224, doi: 10.1007/BF03160612

Nelson D M, Smith Jr W O. 1986. Phytoplankton bloom dynamics of the western Ross Sea ice edge—Ⅱ. Mesoscale cycling of nitrogen and silicon. Deep-Sea Research Part A. Oceanographic Research Papers, 33(10): 1389–1412, doi: 10.1016/0198-0149(86)90042-7

Pan Jianming, Zhao Jun, Li Dong, et al. 2024. Progress of CHINARE on the pattern of Antarctic marine biogenic elements and their ecological and environmental effects. Chinese Journal of Polar Research, 36(3): 329–342, doi: 10.13679/j.jdyj.20240033

Peterson B J, Fry B. 1987. Stable isotopes in ecosystem studies. Annual Review of Ecology and Systematics, 18: 293–320, doi: 10.1146/annurev.es.18.110187.001453

Petrou K, Kranz S A, Trimborn S, et al. 2016. Southern Ocean phytoplankton physiology in a changing climate. Journal of Plant Physiology, 203: 135–150, doi: 10.1016/j.jplph.2016.05.004

Pondaven P, Gallinari M, Chollet S, et al. 2007. Grazing-induced changes in cell wall silicification in a marine diatom. Protist, 158(1): 21–28, doi: 10.1016/j.protis.2006.09.002

Pondaven P, Ragueneau O, Tréguer P, et al. 2000. Resolving the 'opal paradox' in the Southern Ocean. Nature, 405(6783): 168–172, doi: 10.1038/35012046

Post D M. 2002. Using stable isotopes to estimate trophic position: models, methods, and assumptions. Ecology, 83(3): 703–718, doi: 10.1890/0012-9658(2002)083[0703:USITET]2.0.CO;2

Quéguiner B. 2013. Iron fertilization and the structure of planktonic communities in high nutrient regions of the Southern Ocean. Deep-Sea Research Part Ⅱ: Topical Studies in Oceanography, 90: 43–54, doi: 10.1016/j.dsr2.2012.07.024

Raiswell R, Hawkings J, Elsenousy A, et al. 2018. Iron in glacial systems: speciation, reactivity, freezing behavior, and alteration during transport. Frontiers in Earth Science, 6: 222, doi: 10.3389/feart.2018.00222

Reigstad M, Wassmann P. 2007. Does *Phaeocystis* spp. contribute significantly to vertical export of organic carbon?. In: Leeuwe M A, Stefels J, Belviso S, et al, eds. *Phaeocystis*, Major Link in the Biogeochemical Cycling of Climate-Relevant Elements. Dordrecht: Springer, 217–234, doi: 10.1007/978-1-4020-6214-8_16

Rembauville M, Blain S, Armand L, et al. 2015. Export fluxes in a naturally iron-fertilized area of the Southern Ocean–part 2: importance of diatom resting spores and faecal pellets for export. Biogeosciences, 12(11): 3171–3195, doi: 10.5194/bg-12-3171-2015

Rembauville M, Manno C, Tarling G A, et al. 2016. Strong contribution of diatom resting spores to deep-sea carbon transfer in naturally iron-fertilized waters downstream of South Georgia. Deep-Sea Research Part Ⅰ: Oceanographic Research Papers, 115: 22–35, doi: 10.1016/j.dsr.2016.05.002

Roach L A, Smith M M, Herman A, et al. 2025. Physics of the seasonal sea ice zone. Annual Review of Marine Science, 17: 355–379, doi: 10.1146/annurev-marine-121422-015323

Roden N P, Shadwick E H, Tilbrook B, et al. 2013. Annual cycle of carbonate chemistry and decadal change in coastal Prydz Bay, East Antarctica. Marine Chemistry, 155: 135–147, doi: 10.1016/j.marchem.2013.06.006

Roden N P, Tilbrook B, Trull T W, et al. 2016. Carbon cycling dynamics in the seasonal sea-ice zone of East Antarctica. Journal of Geophysical Research: Oceans, 121(12): 8749–8769, doi: 10.1002/2016jc012008

Sallée J B, Matear R J, Rintoul S R, et al. 2012. Localized subduction of anthropogenic carbon dioxide in the Southern Hemisphere oceans. Nature Geoscience, 5(8): 579–584, doi: 10.1038/ngeo1523

Salter I, Kemp A E S, Moore C M, et al. 2012. Diatom resting spore ecology drives enhanced carbon export from a naturally iron-fertilized bloom in the Southern Ocean. Global Biogeochemical Cycles, 26(1): GB1014, doi: 10.1029/2010GB003977

Schmidt K, Atkinson A, Pond D W, et al. 2014. Feeding and overwintering of Antarctic krill across its major habitats: the role of sea ice cover, water depth, and phytoplankton abundance. Limnology and Oceanography, 59(1): 17–36, doi: 10.4319/lo.2014.59.1.0017

Shi Jiuxin, Cheng Yaoyao, Jiao Yutian, et al. 2011. Supercooled water in austral summer in Prydz Bay, Antarctica. Chinese Journal of Oceanology and Limnology, 29(2): 427–437, doi: 10.1007/s00343-010-0011-5

Sigman D M, Altabet M A, McCorkle D C, et al. 1999. The $\delta^{15}N$ of nitrate in the Southern Ocean: consumption of nitrate in surface waters. Global Biogeochemical Cycles, 13(4): 1149–1166, doi: 10.1029/1999GB900038

Skerratt J H, Nichols P D, McMeekin T A, et al. 1995. Seasonal and inter-annual changes in planktonic biomass and community structure in eastern Antarctica using signature lipids. Marine Chemistry, 51(2): 93–113, doi: 10.1016/0304-4203(95)00047-U

Takeda S. 1998. Influence of iron availability on nutrient consumption ratio of diatoms in oceanic waters. Nature, 393(6687): 774–777, doi: 10.1038/31674

Taylor F, McMinn A, Franklin D. 1997. Distribution of diatoms in surface sediments of Prydz Bay, Antarctica. Marine Micropaleontology, 32(3–4): 209–229, doi: 10.1016/S0377-8398(97)00021-2

Thunell R C. 1998. Seasonal and annual variability in particle fluxes in the Gulf of California: a response to climate forcing. Deep-Sea Research Part Ⅰ: Oceanographic Research Papers, 45(12): 2059–2083, doi: 10.1016/S0967-0637(98)00053-3

Trinh R, Ducklow H W, Steinberg D K, et al. 2023. Krill body size drives particulate organic carbon export in West Antarctica. Nature, 618(7965): 526–530, doi: 10.1038/s41586-023-06041-4

Vaz R A N, Lennon G W. 1996. Physical oceanography of the Prydz Bay region of Antarctic waters. Deep-Sea Research Part Ⅰ: Oceanographic Research Papers, 43(5): 603–641, doi: 10.1016/0967-0637(96)00028-3

Volk T, Hoffert M I. 1985. Ocean carbon pumps: analysis of

relative strengths and efficiencies in ocean-driven atmospheric CO_2 changes. In: Sundquist E T, Broecker W S, eds. The Carbon Cycle and Atmospheric CO_2: Natural Variations Archean to Present. American Geophysical Union, 99–110, doi: 10.1029/GM032p0099

Williams G D, Nicol S, Aoki S, et al. 2010. Surface oceanography of BROKE-West, along the Antarctic margin of the south-west Indian Ocean (30–80°E). Deep-Sea Research Part Ⅱ: Topical Studies in Oceanography, 57(9–10): 738–757, doi: 10.1016/j.dsr2.2009.04.020

Williams G D, Nicol S, Raymond B, et al. 2008. Summertime mixed layer development in the marginal sea ice zone off the Mawson coast, East Antarctica. Deep-Sea Research Part Ⅱ: Topical Studies in Oceanography, 55(3–4): 365–376, doi: 10.1016/j.dsr2.2007.11.007

Wilson J D, Barker S, Ridgwell A. 2012. Assessment of the spatial variability in particulate organic matter and mineral sinking fluxes in the ocean interior: Implications for the ballast hypothesis. Global Biogeochemical Cycles, 26(4): GB4011, doi: 10.1029/2012GB004398

Yang Guang, Li Chaolun, Sun Song, et al. 2013. Feeding of dominant zooplankton in Prydz Bay, Antarctica, during austral spring/summer: food availability and species responses. Polar Biology, 36(11): 1701–1707, doi: 10.1007/s00300-013-1387-4

Yu Jianchun, Zhu Guoping, Wang Yinghui, et al. 2023. Sea ice melting drives substantial change in dissolved organic matter in surface water off Prydz Bay, East Antarctic. Journal of Geophysical Research: Biogeosciences, 128(3): e2023JG007415, doi: 10.1029/2023JG007415

Zhang Haifeng, Wang Rujian, Han Zhengbing, et al. 2023. Seasonal variations of siliceous microplankton fluxes and radiolarian assemblages linked to environmental conditions in Prydz Bay polynya, eastern Antarctica. Frontiers in Marine Science, 10: 1135900, doi: 10.3389/fmars.2023.1135900

Zhang Run, Zheng Minfang, Chen Min, et al. 2014. An isotopic perspective on the correlation of surface ocean carbon dynamics and sea ice melting in Prydz Bay (Antarctica) during austral summer. Deep-Sea Research Part Ⅰ: Oceanographic Research Papers, 83: 24–33, doi: 10.1016/j.dsr.2013.08.006

Zheng Shaojun, Shi Jiuxin. 2011. The characteristic of sea ice growth and melt in the Prydz Bay region, Antarctica. Periodical of Ocean University of China (in Chinese), 41(7–8): 9–16, doi: 10.3969/j.issn.1672-5174.2011.07.002

Appendix

Table A1. Mean value and uncertainty of TOC, TON, $\delta^{13}C_{org}$, and $\delta^{15}N$ of POM in sediment trap samples of both summers

CHINARE (year)	Cup	TOC proportion/%	TON proportion/%	$\delta^{13}C_{org}$/‰	$\delta^{15}N$/‰
CHINARE-36 (2019/2020)	#1	10.19 ± 0.04	1.25 ± 0.07	–25.4	1.8 ± 0.0
	#2	13.13 ± 0.06	1.55 ± 0.01	–27.6	2.1
	#3	10.72 ± 0.02	1.56 ± 0.03	–26.9	3.4
	#4	11.11 ± 0.02	1.61 ± 0.02	–28.7	3.5
	#5	10.33 ± 0.04	1.56 ± 0.02	–29.7 ± 0.1	3.0 ± 0.0
	#6	8.76 ± 0.03	1.24 ± 0.00	8.27	2.2 ± 0.2
	#7	6.87 ± 0.01	0.94 ± 0.02	7.75	3.0
CHINARE-37 (2020/2021)	#1′	11.78 ± 0.04	1.32 ± 0.00	–30.6	1.0
	#2′	9.98 ± 0.06	1.06 ± 0.00	–30.5	0.9
	#3′	7.95 ± 0.04	0.95 ± 0.01	–29.9	0.8 ± 0.1
	#4′	6.67 ± 0.03	0.77 ± 0.01	–29.0	1.3
	#5′	5.61 ± 0.05	0.70 ± 0.00	–27.8	1.5
	#6′	5.25 ± 0.01	0.69 ± 0.00	–27.5	1.6

Note: For TOC and TON analysis, every sample was measured twice at one time, and the mean of two measurements is reported here. For $\delta^{13}C_{org}$ and $\delta^{15}N$ analysis, every sample was measured once, and some samples were randomly selected for replicate testing.